CHAPTER 4. Long term Temporal and Spectral Variations of Cen X-3

4.1 Introduction

The X-ray light curves of X-ray binaries reveal many different aspects of these system. In the preceding chapters we have seen how these light curves were used to determine the orbital elements of the neutron star orbit. The variations of the orbit elements with time give us information about time evolution of the system. All these studies of X-ray binaries are possible because we can see and measure the variations in the X-ray light curves with the help of our X-ray detectors. These light curves of X-ray pulsars show periodic variations on times scales of few milliseconds to few hours due to spin of the neutron star when the light curve is seen with a fine enough time resolution. The same light curve at a more coarse time resolution but with a longer stretch may show variations due to variable absorption of X-rays at different orbital phase. Variations due to varying absorption in the neutron star binary are periodic in nature and span over a time scale of few minutes to several days. Many sources also show quasi periodic variations in their X-ray light curves at timescales smaller than the neutron star orbital period which are believed to arise due to some material inhomogeneity orbiting the neutron star and blocking the X-rays in the line of sight of the observer. These variations are called Quasi Periodic Oscillations (QPOs). QPOs in X-ray binaries are observed between a frequency range of few millihertz to few kilohertz. Now if a system is observed at an even coarser time resolution, of say one day, but for a very long time , say like a few months, as the All Sky Monitor (ASM) on board RXTE does, then the light curves of the same sources may reveal variations of time scales greater than the orbital period of the neutron star. These variations are termed as superorbital variations and they can be periodic, aperiodic or quasi periodic in nature differing from source to source. In this chapter we will be discussing the

superorbital variations seen in the X-ray light curve of the persistent HMXB pulsar Cen X-3.

To demonstrate the variations seen in X-ray light curves described above, we have chosen the light curves of SMC X-1 as an example. The light curves of SMC X-1 show spin period variations at a period of 0.71 s (Figure 4.1), orbital period variations at period of 3.88 days (Figure 4.2) and quasi periodic superorbital variations (Fig 4.3). The quasi periodic superorbital variations of SMC X-1 are in the range of 50-70 d (Grubers & Rothschild 1984; Clarkson et al. 2003, Wen et al. 2006). Sources which have periodic superorbital variations are Her X-1 (Tananbaum et. al. 1972, Still & Boyd 2004), LMC X-4 (30.28 d: Paul & Kitamoto 2002), 2S 0114+650 (30.75 d: Farrell, Sood & O'Neill 2006), SS 433 (164 d: Eikenberry et al. 2001; Fabrika 2004), XTE J1716–389 (99.1 d: Cornelisse, Charles & Robertson 2006), 4U 1820–303 (172 d: Smale & Lochner 1992; Zdziarski et al. 2007a) and Cyg X-1 (150 d: Kitamoto et al. 2000; Lachowicz et al. 2006). Among these sources Her X-1, LMC X-4 and 2S0114+650 are accretion powered pulsars. There are other X-ray binaries that show quasi periodic long term intensity variations like SMC X-1. GRS 1747-312 shows quasi periodic intensity variations of $\sim$ 150 d (inć Zand et al. 2003; Wen et al. 2006). Cyg X-2 has quasi periodic long term variability with period in the range of 60-90 d (Smale & Lochner 1992; Paul, Kitamoto & Makino 2000) and LMC X-3 also shows long term intensity variations with periodicity in the range of 100-500 d (Wen et al. 2006) that is unstable over a longer period (Paul et al. 2000; Wen et al. 2006) Long term quasi periodic variations with a period of about 217 d are also seen from the Rapid Burster (X1730–333) which is in the form of recurrent outburst rather than a gradual change in X-ray intensity (Masetti 2002). Refer Wen et al (2002) for a detailed review of superorbital variations in X-ray binaries.

Periodic long term variations are explained as obscuration of the central X-ray source by an accretion disk inclined with respect to the orbital plane. Figure 4.4 shows a configuration in which a tilted accretion disk is blocking the central X-ray source. A precession of this accretion disk will block the X-rays from the central source periodically and hence introduce long term periodic variability in the X-ray light curve as seen by a distant observer. Many mechanisms such as tidal interaction of the inclined disk with the companion star (Katz 1073) and precession

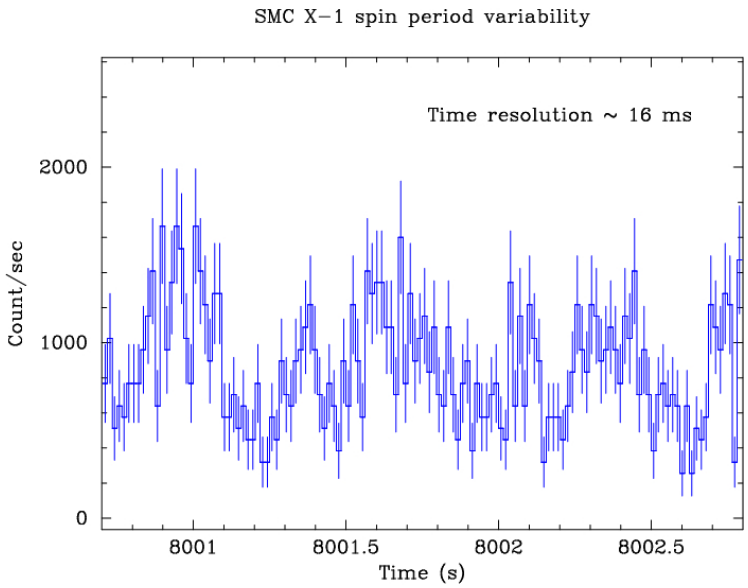

Figure 4.1 RXTE-PCA light curve of SMC X-1 binned with 16 ms time resolution. The 0.71 s spin period is clearly visible.

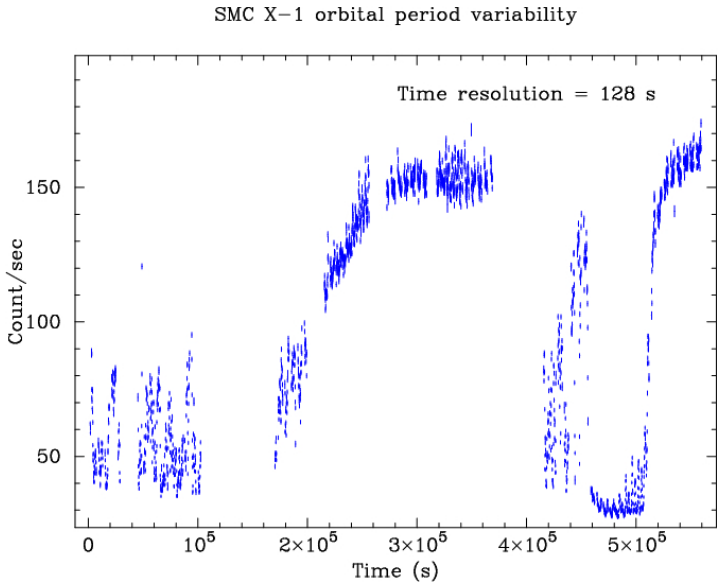

Figure 4.2 RXTE-PCA light curve of SMC X-1 binned with 128 s time resolution. The 3.88 d orbital period variability is clear. The almost zero counts for time between 4.06×10^4 s to 5×10^4 s is due to eclipse of X-ray pulsar by the companion star.

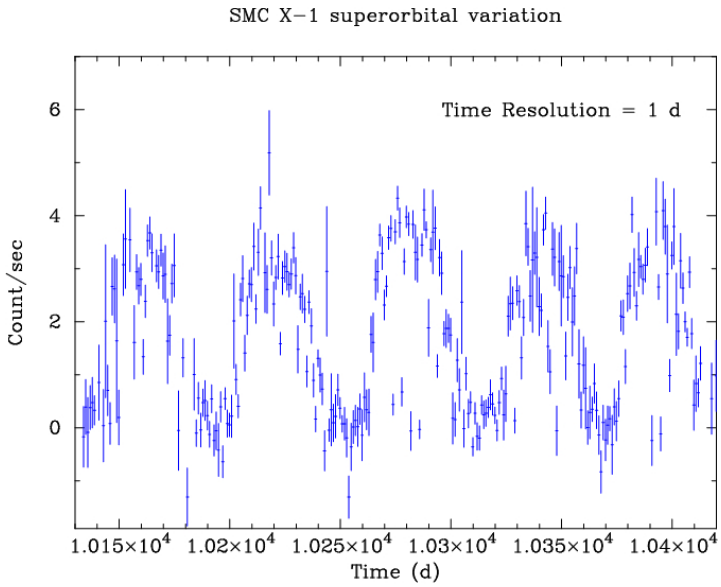

Figure 4.3 ASM light curve of SMC X-1 binned with 1 day time resolution. Five cycles of the 50-70 day superorbital quasi-periodic variation are shown.

of rotation axis of the companion star due to its inclination with respect to the orbital plane, causing a slaved precession of the disk (Roberts 1974) have been proposed to explain precession of the disk. Attempts have been made to explain the 35 days periodicity seen in Her X-1 arising due to interaction of the inner accretion disk and the rotating magnetic dipole of the neutron star (Truemper et al. 1986). An inclined disk will try to align the inner accretion disk along the neutron stars rotational equator. If the neutron star is precessing then the inner accretion disk will also precess accordingly trying to align itself along the rotational equator and can explain the periodic variability in the light curve (Lipunov, Semenov & Shakura 1981).

Many mechanisms have also been proposed to generate twisted, warped and/or tilted accretion disks. One of them is a tilted accretion disk produced due to coronal winds (Schandl & Meyer 1994 ;Schandl 1996). In this model X-rays from the neutron star irradiate the accretion disk producing a hot corona which in the vicinity of the inner disk radii is hydrostatically layered. In the vicinity of the outer disk, sound velocity of the hot coronal gas exceeds the escape velocity in the gravitational potential hence forming a coronal wind. The matter leaving the binary system will exert repulsive forced on the disk. This will tilt and twist the accretion

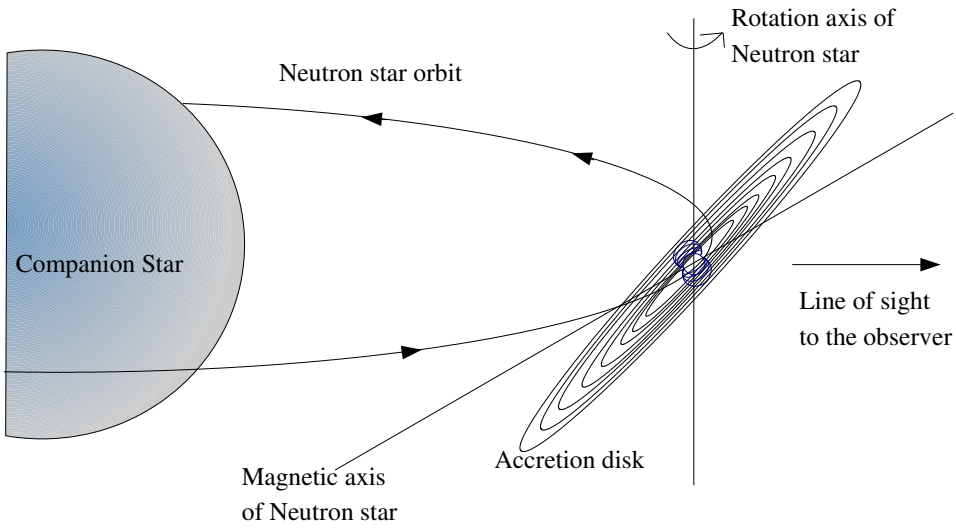

Figure 4.4 Figure shows a tilted accretion disk blocking the central X-ray source from the line of sight of the observer. A precession of this disk would introduce periodic variability in the light curve as recorded by a distant observer. Note Figure not to scale.

disk which will then lead to a complex irradiation of the disk surface. Some regions of the disk will be directly illuminated while other regions may be shadowed either by the disk itself or the optically thick corona in the inner regions. Also the strength of coronal wind will depend on the incident X-ray flux and hence will be variable. The sum total of all this is that a net repulsive torque is maintained which will keep the accretion disk tilted and twisted. Figure 4.5 shows a simulated disk structure produced to explain the 35 day period of Her X-1. It is twisted and tilted at an angle of 80^0 and has a precession period of 35 d. Figure is taken from Schandl & Meyer (1994).

Radiation pressure will give rise to a net torque in a warped accretion disc which is optically thick to absorption and reemission of incident radiation. (Petterson 1977, Maloney, Begelman & Pringle 1996, Wijers & Pringle 1999, Ogilvie & Dabus 2001). This can be understood as follows. Consider an annulus of accretion disk with a central source of radiation. If the annulus is slightly warped, it will be illuminated by the central source and if the disk is optically thick, it will absorb the incident flux. The momentum associated with this absorption is purely radial and hence the force due to incident radiation is will produce zero torque. If the disk is optically

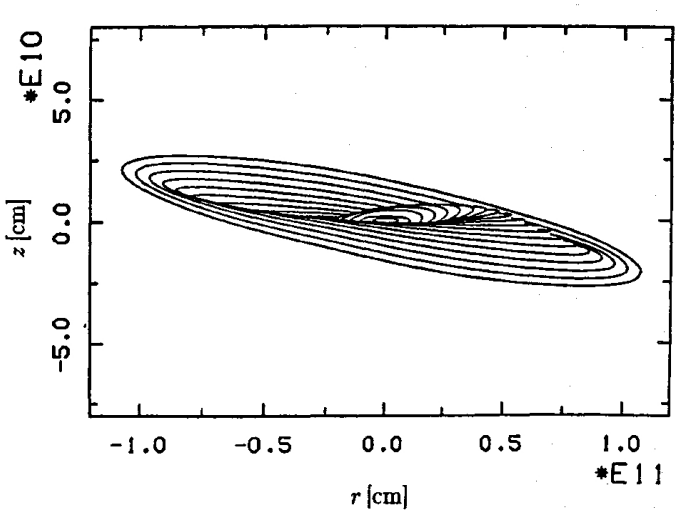

Figure 4.5 Figure shows tilted and twisted accretion disk (Schandl & Meyer 1994).

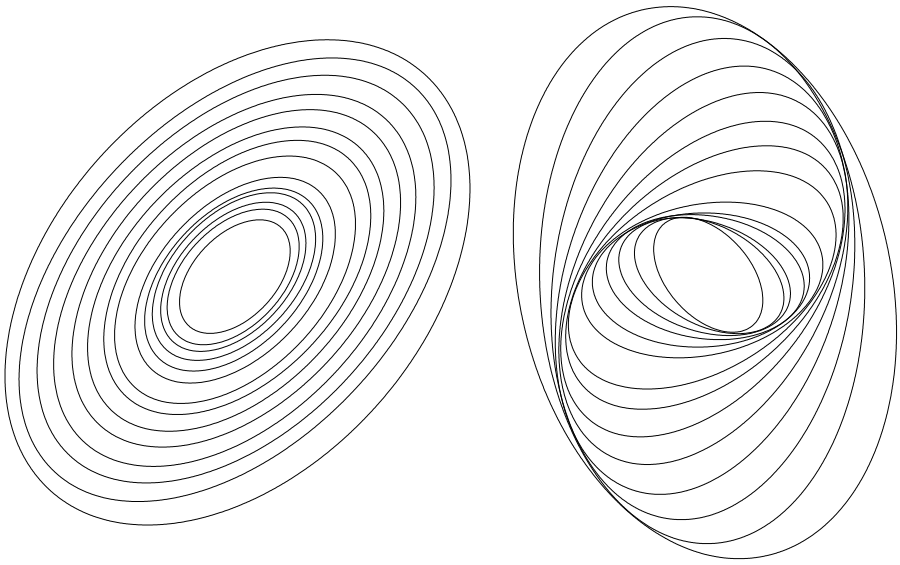

Figure 4.6 A previously tilted accretion disk (left hand side Figure) develops warps (right hand side Figure) due to differential precession because of tidal interaction between the disk rings and the companion star.

thick to reemission of the absorbed radiation, then both the net emitted flux and the radiation pressure due to it will be normal to the local plane of the disk. This radiation pressure due to reemission radiation which is acting on the irradiated surface will exert a torque at each exposed point of the annulus. Since the annulus is warped the radiation momentum per unit area of the ring will be non-asymmetric producing a net torque on the ring. Pringle (1996) has shown that even initially planar disks are unstable to warping due to radiation pressure. Iping and Petterson (1990) have done detailed numerical simulations of centrally illuminated tilted and twisted accretion disks. They have shown that precession of such disks can deviate substantially from being purely periodic. The main results of their paper are firstly, tidal interactions between disk rings and the companion star lead to precession of inclined rings, the frequency of which depends on the radius of the ring. Thus the outer ring of an accretion disk will precess the fastest. This differential precession gradually twists the disk. Figure 4.6 illustrates this point. Secondly, when the disk is twisted, the illumination by the central X-ray source is complicated by shadowing effects which depends on the warp shape. This can make the rings precess in either direction and also change their inclination angle. Finally, the mass stream from the inner Lagrangian point feeds into the outermost ring and mixes with the material of that ring. Since this stream lies in the binary plane or close to it, it will tend to move the plane of the outermost ring towards the binary plane.

Presence of a third body in the system which will modify the accretion rate of matter onto the X-ray source have also been used to explain the observed superorbital modulation in X-ray light curve (Zdziarski, Wen & Gierlinski 2007).

In this chapter we talk about the superorbital variations of Cen X-3. As we already know Cen X-3 is a high mass X-ray binary pulsar with a 4.81 s spin period and a 2.08 days orbital period. It is monitored by the All Sky monitor on board RXTE. The multi band X-ray light curves of Cen X-3 obtained by RXTE-ASM show many episodes of high and low X-ray intensities. It is seen that the high intensity phases last between a few to upto 110 days and the separation between two high intensity phases also varies widely. One remarkable feature of this source is that during its high intensity phases it occupies two very distinct spectral states.

When the source makes a transition from the low intensity phase to the high intensity phase, it adopts one of these two spectral states and during the entire high intensity phase it remains in that particular spectral state. During December 2000 to April 2004, all the high intensity episodes showed a hardness ratio which is significantly larger than the same during all the high states prior to and subsequent to this period. It is also found that most of the soft outbursts reach a nearly constant peak flux in the 5-12 keV band. The details of this study of Cen X-3 is covered in section 3 of this chapter.

To understand these variabilities in the X-ray light curve of Cen X-3 we looked at the orbital modulation and pulsed fraction in different intensity states. In the high state, the eclipse ingress and eclipse egress are found to be sharp whereas in the intermediate state the transitions are more gradual. In the low state, instead of eclipse ingress and egress, the light curve shows a smooth intensity variation with orbital phase. This is compared with the intensity dependant orbital modulation of Her X-1, SMC X-1 and LMC X-4. We also see that the pulsed fraction of Cen X-3 is intensity dependant. This dependance is similar to that seen in SMC X-1. We will discuss the details of this study in Section 4 of this chapter.

We have also investigated properties of the Quasi Periodic Oscillation (QPO) features in Cen X-3 over a period of about four years. The observations cover a wide range of X-ray intensity of the source in excess of the binary intensity modulation. We have detected QPOs in 11 out of a total 81 pointings with the PCA with RMS intensity fluctuation upto 10%. The results from the study of QPOs of Cen X-3 are presented in details in section 5 of this chapter. The next section describes some instrumental aspects of ASM relevant to our work.

4.2 Some details of All Sky Monitor on board Rossi X-ray Timing Explorer

Much of the work presented in this chapter is done using the light curves provided by All Sky Monitor. ASM monitors all the known X-ray binary pulsars regularly and provides long term light curves in four energy bands namely, 1.5-3, 3-5, 5-12, and the light curve produced from the full energy range of 1.5-12 keV (Levine et al. 1996). This All Sky Monitor consists

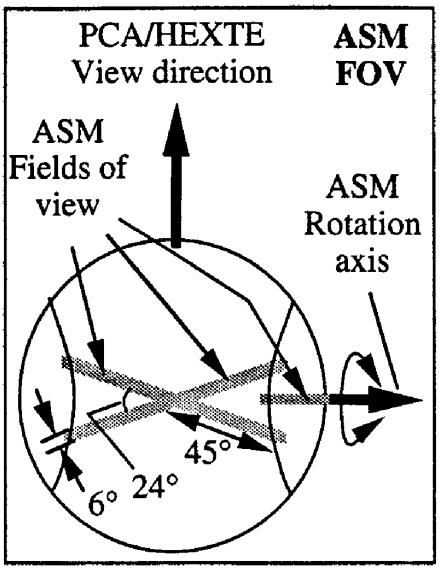

Figure 4.7 The FOV of the three SSCs are indicated. The centers of the FOV of SSC 1 and SSC 2 are approximately co-aligned perpendicular to the ASM rotation axis. The center of the FOV of SSC3 is pointed parallel to the rotation axis. The view direction of the other two RXTE instruments is indicated. Figure taken from Levine et al. 1996

of three scanning shadow cameras (SSC) mounted about a single rotation axis. Two of these three SSCs, SSC1 and SSC2 have their field of view (FOV) perpendicular to the rotation axis and the third SSC, SSC3 has its FOV parallel to the rotation axis. Thus the three detectors of ASM have different viewing orientation. They make intensity image of a large part of the sky with a few arc minute angular resolution for every rotation around the ASM rotation axis. Figure 1.7 of the first chapter and Figure 4.7 shows the different orientations and different FOV of the three ASM cameras.

4.3 Aperiodic intensity variations and accretion mode changes in Cen X-3

We study long term aperiodic variations in the X-ray light curve and the associated spectral variations in Cen X-3 using the multi band per dwell light curves provided by All Sky Monitor. The long term characteristics of Cen X-3 light curve are compared with the characteristics of three other bright X-ray binary pulsars, namely Her X-1, Vela X-1 and SMC X-1. Observations

of all the four sources cover the period from 5th January 1996 to 12th May 2005.

All the four sources studied here have orbital periods in the range of 1.7 d to 8.9 d and show long lasting eclipses during which the X-ray intensity decreases by a large factor (see Table 4.1). Some residual X-ray emission is seen during the eclipse of the central X-ray source which is due to reprocessing of pulsar X-rays by the stellar wind of the companion star. Therefore we removed all eclipse data before further analysis which otherwise would have contaminated the measurement of averaged X-ray intensity. The procedure to this is described below.

The orbital period, mid-eclipse time and eclipse duration were first derived for each source from the unfiltered ASM light curves. Table 4.1 gives these values for each of the four sources. The orbital periods derived here are consistent with those derived by analysing the pulse arrival times. We note here that since the eclipses seen in these sources are asymmetric in nature, the measured mid-eclipse times are not very accurate and hence should not be used to study the orbital evolution of the binary. The eclipse durations given in Table 4.1 also include the eclipse ingress and egress times.

Table 4.1 Orbital parameters of the four sources derived from RXTE-ASM light curves

Source name	Orbital period (day)	Mid-eclipse time (MJD)	Eclipse duration in orbital phase with ingress and egress included
Cen X-3	2.08702(3)	50087.295(1)	0.306
Her X-1	1.70016(1)	50088.236(3)	0.318
Vela X-1	3.8920(1)	50087.286(6)	0.231
SMC X-1	8.9646(3)	50087.542(4)	0.377

To filter the eclipse data, individual light curves of each source were folded with the respective orbital period derived and the orbital phase of the eclipse ingress and egress along with the epoch of folding were noted. All the data points falling within the eclipse ingress and egress phases were removed to get the eclipse subtracted X-ray light curve.

As explained in the previous section, due to different FOV and viewing orientations of the three ASM detectors, light curve from each of them may have different effective exposure for any given X-ray source in their field of view. In addition to this another issue is that one

of the detectors is known to have a slightly different energy calibration (A. Levine, private communication). Such differences can produce artificial spectral variations in the observed X-ray light curves. To avoid the confusion that observed spectral variations may or may not be instrumental artifacts, all the analysis presented here was also done separately for each ASM detector. The results thus obtained from each detector are similar to those obtained from a combined light curve generated using data from all the detectors. Here we present only the results obtained by a combined light curve.

Spectral evolution study of Cen X-3 was done using two harness ratios HR1 and HR2. Hardness ratio is defined as the ratio of X-ray intensity in higher energy band to the X-ray intensity in the lower energy band. For the work presented here, the two hardness ratios were defined as $HR1 = (3-5)keV/(1.5-3)keV$ and $HR2 = (5-12)keV/(3-5)keV$. Hardness ratio for data points falling during the eclipse times were not calculated. As will be detailed later, Cen X-3 shows significant spectral state changes. To ensure that these spectral mode changes in Cen X-3 are not an artifact of changing energy calibration of the ASM detectors, the multi band ASM light curves of Her X-1, Vela X-1 and SMC X-1 were also analysed in the same way as the Cen X-3 light curve were analysed and used for comparison.

4.3.1 Results

Eclipse subtracted RXTE-ASM light curves of Cen X-3 in the three energy bands are shown in Figure 4.8. The light curve shows wide variability in the X-ray luminosity. The source frequently switches between low and high states with intensity varying by a large factor. In all the three energy bands the peak flux during the bursts is larger compared to the low state flux by upto a factor of 40. The low and high intensity states last between a few to upto 110 days and occur with no apparent periodicity. The X-ray flux during the low states averaged over a few days is always found to be within about 30% of the average low state flux of the entire observation period. Period searches with different algorithms do not show any long term periodicity in the intensity variation of Cen X-3. A plot of the power spectrum of ASM light curve is shown in Figure 4.9. The only peak seen at 5.5 μHz in the power spectrum is due to

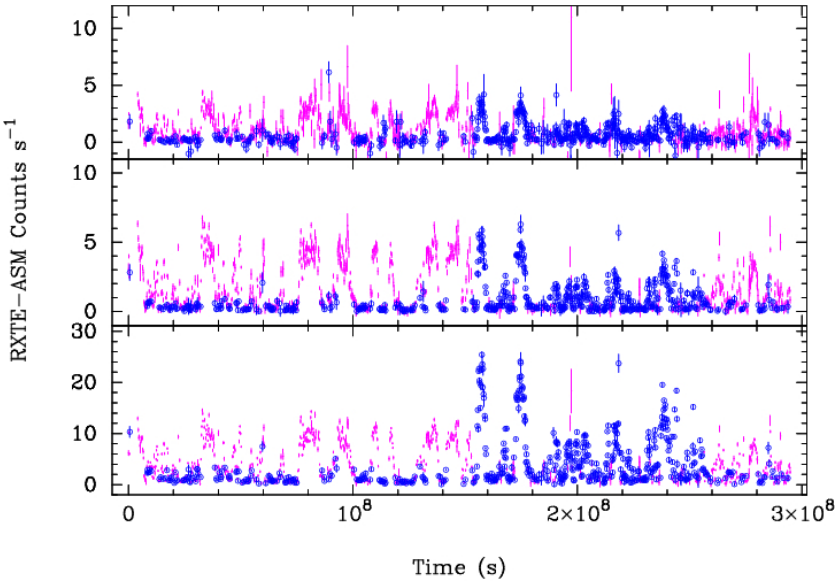

Figure 4.8 RXTE-ASM light curves of Cen X-3 in three different energy bands of 1.5-3 keV, 3-5 keV and 5-12 keV are shown here in top, middle and bottom panels respectively. Blue circles are used for data points with hardness ratio (between 5-12 keV and 3-5 keV count rates) greater than 3.5

the orbital motion of the neutron star. No other periodic or quasi periodic signals are seen in the power spectrum.

Other high mass X-ray binary pulsars that show superorbital intensity variations in their X-ray light curve have smooth and almost sinusoidal variations over the superorbital period. Her X-1 shows prominent stable superorbital intensity variations when it is out of the occasional anomalous low states (Still & Boyd 2004). Each superorbital period of Her X-1 consists of one main-on phase and one short-on phase separated by two low intensity phases. Figure 4.10 shows eclipse subtracted ASM light curves of Her X-1, Vela X-1 and SMC X-1. The Her X-1 and SMC X-1 which are known to show periodic and quasi periodic superorbital intensity variations respectively show smooth transitions from high state to low state. But when these light curves are compared to the Cen X-3 light curves in Figure 4.8 the sharp rise and fall in intensity around the high states which last about 2-8 days stand out in stark contrast.

Examining the coarse spectral evolution of Cen X-3 as it went though its intensity changes revealed significant spectral state changes during the ASM observations from 5th January 1996

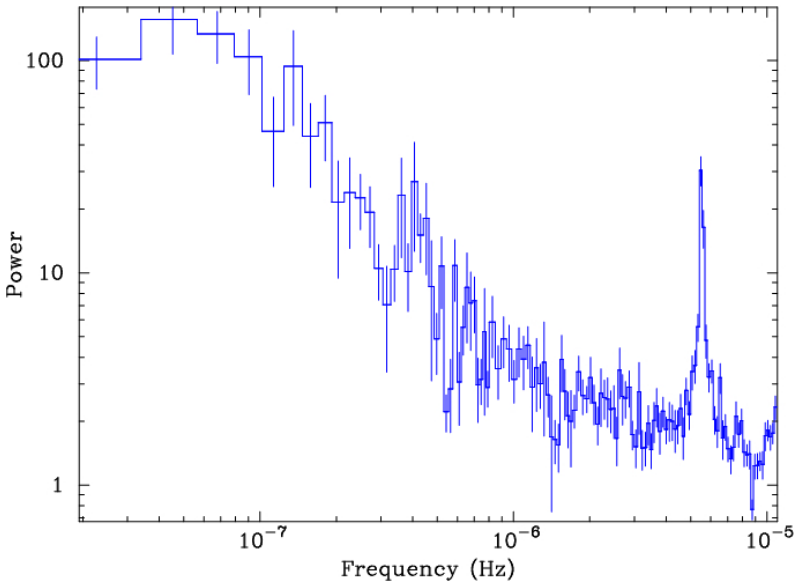

Figure 4.9 Power spectrum of RXTE-ASM light curves of Cen X-3 is shown. The power spectrum shows a peak at 5.5 μHz due to the orbital motion of the neutron star.

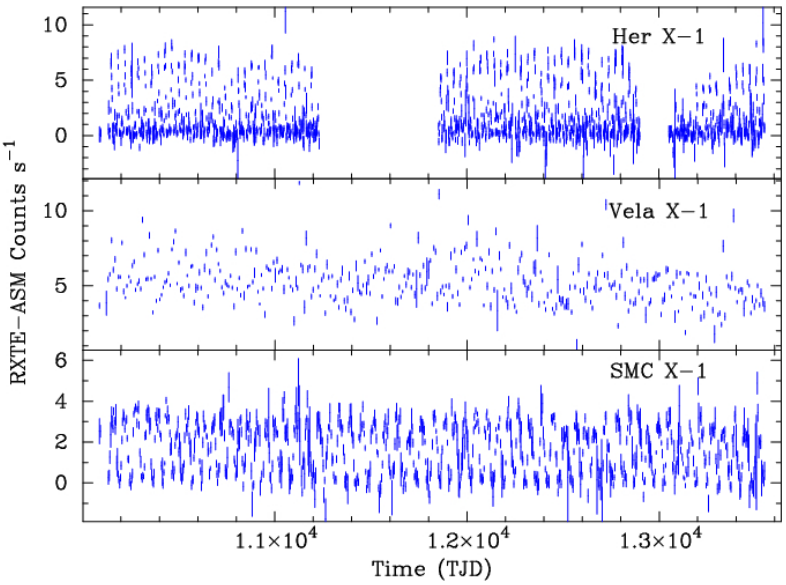

Figure 4.10 The 1.5-12 keV RXTE-ASM light curve of Her X-1, Vela X-1 and SMC X-1 are plotted in the top, middle and bottom panels respectively. For Her X-1, data obtained during the two anomalous low states were omitted.

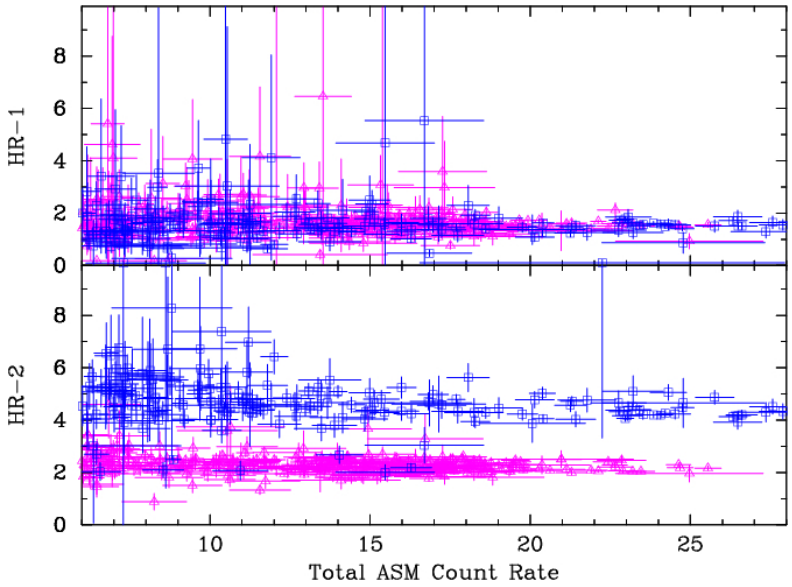

Figure 4.11 The two hardness ratios HR-1 and HR-2 derived from the RXTE-ASM light curves of Cen X-3 are plotted here against the ASM count rate for value greater than 2 per second. Data points obtained between MJD 51800 and 53100 are shown in blue.

to 12 May, 2005. A plot of HR1 and HR2 against the total ASM count rate is shown in Figure 4.11. During the low states, the hardness ratio measurements have large error bars. So in fig 4.11 we have plotted only the data points during which the average ASM count rate is more than 2. The hardness ratio measured during the high states clearly shows a change in spectral shape of the source in the period between December 2000 (TJD 11800) and April 2004 (TJD 13100). A plot of the medium energy (3-5 keV) X-ray count rate against the hard X-ray (5-12 keV) count rate very clearly shows the existence of two different spectral states in Cen X-3 (Fig 4.12). The data points that fall between TJD 11800 and TJD 13100 are marked in blue clearly bringing out the fact that data points belonging to the two arms in fig 4.12 are from different time ranges.

Figure 4.12 plots the 1.5-3 keV and 3-5 keV light curve against the 5-12 keV light curve. The two branches seen in this Figure are due to the changing spectral state of Cen X-3.

Figure 4.13 is a plot of low energy (1.5-3.0 keV) and medium energy (3-5 keV) X-ray count rate against the hard X-ray (5-12 keV) count rate of the three sources, Her X-1, Vela X-1 and

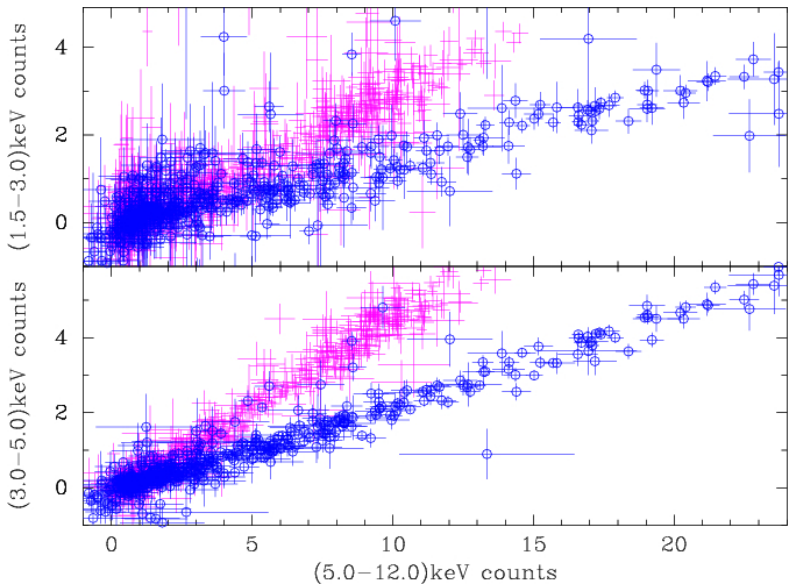

Figure 4.12 The RXTE-ASM count rates of Cen X-3 in soft (1.5-3 keV) and medium (3-5 keV) energy bands are plotted against the hard (5-12 keV) X-ray count rate. Data obtained between TJD 11800 and TJD 13100 are shown as blue circles.

SMC X-1. No spectral evolution as is evident from these Figures for these sources. Count rates in the medium and hard X-ray appear to be very well correlated for Her X-1 and SMC X-1, while for Vela X-1 there is significant scatter. In the Figure the blue points belong to the period between TJD 11800 and TJD 13100. This clearly rules out the possibility that the changes in the hardness ratio detected in Cen X-3 between December 2000 to April 2004 are produced artificially due to any change in energy gain calibration of the detector system.

Another interesting feature of the Cen X-3 light curve prior to December 2000 (TJD 11880) is that there appears to be a ceiling in the maximum luminosity that the source reaches during the outbursts. The ceiling is most clearly visible in the 5-12 keV band and seems to be present in the 3-5 keV band as well.

4.4 Understanding the Intensity states of Cen X-3

To understand the phenomenon leading to the aperiodic variations in Cen X-3 light curves we study orbital modulation of X-ray light curves as a function of source intensity. We also study the dependence of pulsed fraction on the source intensity. The motivation for this work

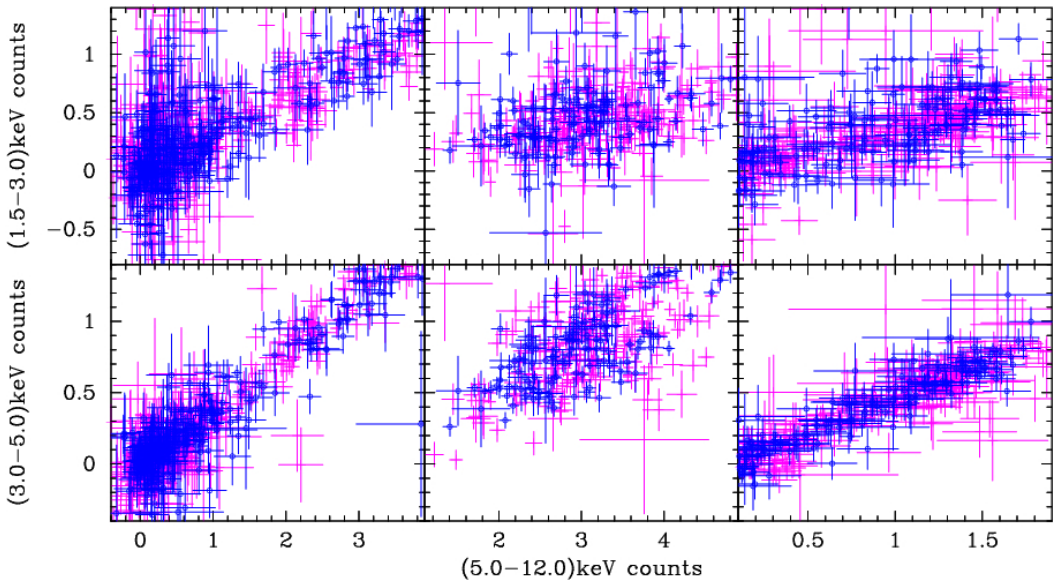

Figure 4.13 The RXTE-ASM count rates in soft (1.5-3 keV) and medium (3-5 keV) energy bands are plotted against the hard (5-12 keV) X-ray count rates for the three sources Her X-1, Vela X-1 and SMC X-1. As in Fig 4.11, data obtained between MJD 51800 and 53100 are shown as circles. The error bars are not shown for the sake of clarity.

comes from previous studies of Her X-1, SMC X-1 and LMC X-4 done by other authors. These three sources, as mentioned earlier, show superorbital intensity variations in their long term light curves. Her X-1 and LMC X-4 show periodic variations at time scales of 35 days and 30.5 days respectively whereas SMC X-1 shows quasi periodic variations at 50-60 days time scale. The super orbital variations seen in these sources are explained as arising due to obscuration of the central X-ray source by a warped precessing accretion disk. Scott & Leahy (1999) found using a subset of RXTE-ASM light curve of Her X-1 that the orbital modulation is shallower in the short-on state compared to the same in the main-on state. Also in the *BeppoSAX* observations of LMC X-4, the absence of clear eclipse transitions in low state was interpreted as due to obscuration of the central X-ray source by the precessing accretion disk (Naik & Paul 2003). The periodic pulsations due to the spin of the neutron star are not detected in the low state of SMC X-1. This is explained by assuming that total emission from SMC X-1 is composed of two components, one highly variable pulsed component and a second unpulsed component. In the low state, the unpulsed component becomes dominant leading to

non-detection of pulses in low state (Kaur et al. 2007).

Cen X-3 intensity variations are aperiodic in nature which makes one suppose that these variations could be due to a changing mass accretion rate. Long term observations with Burst and Transient Source Experiment (BATSE) of the *Compton Gamma Ray Observatory (CGRO)* found that Cen X-3 has alternate spin-up and spin-down intervals which last from about 10 to 100 days (Finger, Wilson & Fishman 1994). However, *GINGA* observations revealed that there is no correlation between the observed X-ray intensity and pulse period derivative of Cen X-3 (Tsunemi, Kitamoto & Tamura 1996) and it was suggested that the observed X-ray intensity of Cen X-3 does not represent its mass accretion rate. Hence studying the orbital modulation and pulsed fraction of Cen X-3 can shed more light on its aperiodic long term intensity variations.

In this section the orbital modulation of the 1.5-12 keV X-ray flux of Cen X-3 when the source is in high, intermediate and low states is investigated to understand if the aperiodic variations are occurring due to a variable mass accretion rate or due to the variable obscuration of the central X-ray source by an accretion disk. We also study the pulsed fraction of Cen X-3 light curve as a function of the source intensity state. The eclipse structure is useful to know the size of the observed X-ray emission region in different intensity states. The pulsed and total X-ray emission of the source in its different intensity states are measured using the many observations of Cen X-3 by RXTE-PCA. Evolution of the pulsed fraction with the observed X-ray intensity is useful to know the relative importance of scattered X-ray emission in different intensity states.

4.4.1 Orbital modulation at different X-ray intensity states of the source

The 1.5-12 keV ASM light curves of four sources Cen X-3, Her X-1, SMC X-1 and LMC X-4, covering about 4100 days from January 1996 are used to study and compare the orbital modulation of these sources in three different intensity states. The light curves of the four sources binned with their respective orbital periods after excluding the eclipse data are shown in Figure 4.14, for 500 consecutive days. The distinctly aperiodic intensity variation of Cen X-3

is in sharp contrast with the periodic modulation in Her X-1 (with one main-on and one short-on state), LMC X-4 (with smaller signal to noise ratio) and the quasi-periodic modulation in SMC X-1 (with some scatter within each high state).

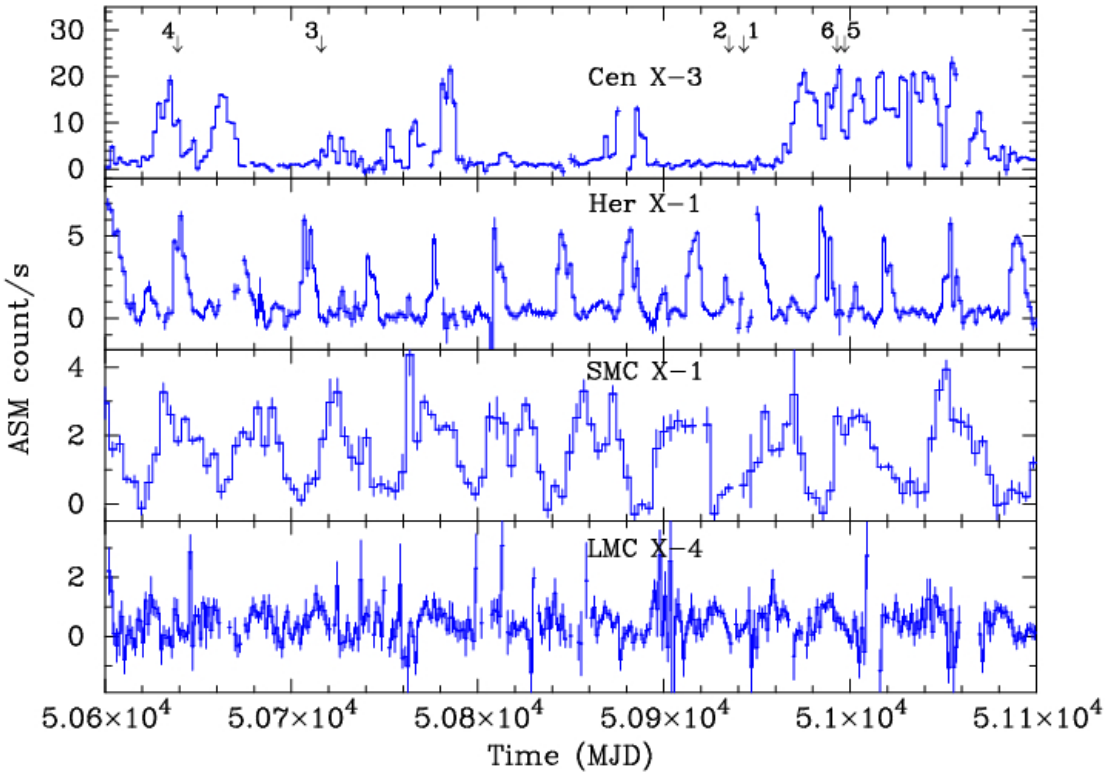

Figure 4.14 The ASM light curves of Cen X-3, Her X-1, SMC X-1 and LMC X-1 are shown here for 500-d binned with the orbital period of the respective sources. The Cen X-3 light curve clearly shows the aperiodic superorbital variations, Her X-1 and LMC X-1 light curves show periodic flux variations whereas SMC X-1 light curve shows quasi-periodic flux variations. The numbered arrows in the Cen X-3 light curve represent the times during which the respective pulse profiles of 4.17 are taken.

The analysis procedure used to make the orbital modulation curves at different intensity states for Cen X-3, Her X-1 and SMC X-1 is same. Only for LMC X-4, a slightly different analysis has been used since its signal to noise ratio is small. The LMC X-4 analysis procedure is hence described separately. The 1.5-12 keV ASM light curves of Cen X-3, Her X-1 and SMC X-1 are first separated into three light curves for each source. The three light curves are for high, intermediate and low intensity states of the respective sources. The orbit averaged count

Table 4.2 The source parameters

Source	Orbital Period[1] (days)	Eclipse Duration (days)	Orbit averaged Count rate for		
			High	Inter-mediate	low
Cen X-3	2.08706 ± 0.00009	0.52	≥ 18.0	$18.0 - 2.0$	≤ 2.0
Her X-1	1.70015 ± 0.00009	0.22	≥ 2.5	$2.5 - 1.0$	≤ 1.0
SMC X-1	3.8921 ± 0.0004	0.62	≥ 1.3	$1.3 - 0.7$	≤ 0.7
LMC X-4[2]	1.40840 ± 0.00006	0.23	-	-	-

[1]Orbital periods are measured from *RXTE*-ASM light curves.
[2]The high, intermediate, and low states of LMC X-4 were determined using the phases of its stable superorbital period. See §2 for details.

rate intervals defining the high, intermediate and low states of each source are given in Table 2. To differentiate the full ASM light curve into light curves for the three intensity states, we first calculated the average count rate per binary orbit after excluding the eclipse data. Procedure used for subtracting the eclipse data is same as described in section 1.2.1. Depending on the average count rate in a binary orbit, the data points available during that orbit were collected in one of the three high, intermediate or low state light curves. These three light curves of each source were then folded with the respective orbital period of the source to get the orbital modulation curves shown in Figure 4.15.

For LMC X-1, the ASM light curve is first folded with the superorbital period. The ephemeris for superorbital modulation is determined as follows.

$$\mathrm{T_{min}[MJD]} = 50092.8 + (30.31 \pm 0.01)N, \tag{4.1}$$

where N is an integer. The high, intermediate and low states are then determined based on the superorbital phase. Data points having superorbital phase between 0.35 to 0.55 belong to high state, those between (0.20 to 0.35, 0.55 to 0.80) belong to intermediate state and low state data points have superorbital phase -0.20 to 0.20, respectively. Depending on the superorbital phase of the data point it is collected in either of the three intensity state light

curve. These three light curves are then folded with the orbital period of LMC X-4 to get the orbital modulation curves.

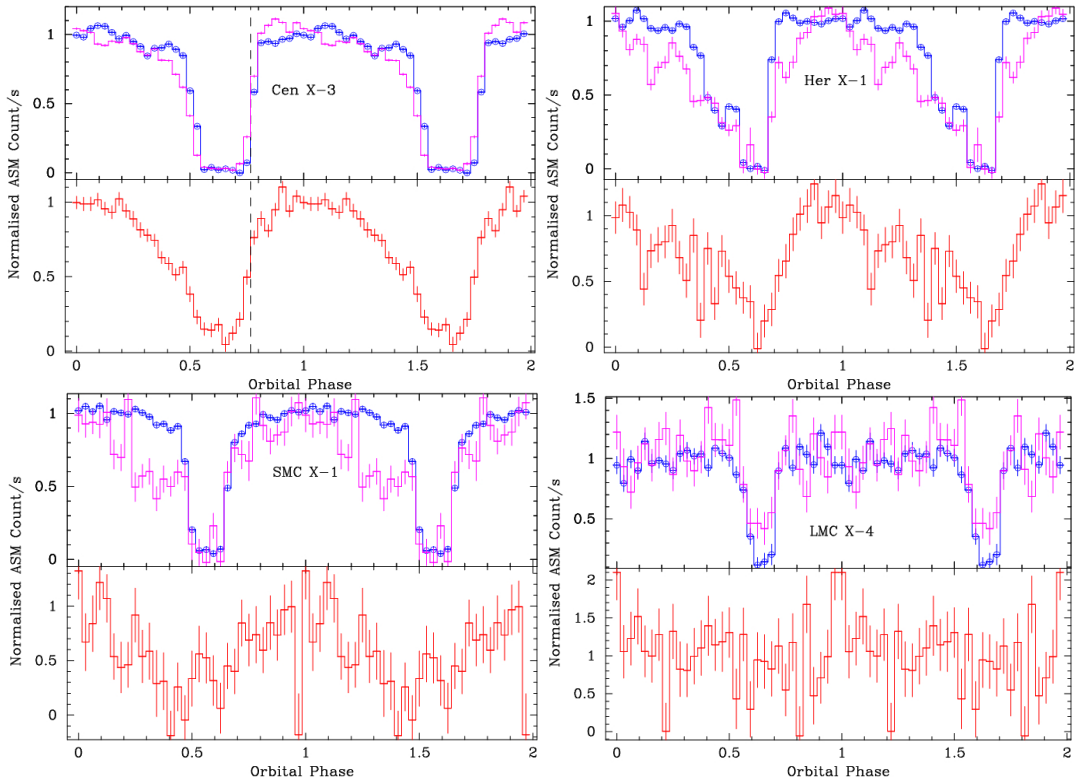

Figure 4.15 The orbital modulation in high, intermediate and low states shown here for four X-ray sources Cen X-3, Her X-1, SMC X-1 and LMC X-4. The high- and intermediate-state plots are shown in the upper panel, with the circles denoting the high--state points. The plot in the lower panel shows the low-state orbital modulation. All the plots are normalized by dividing the original curve with the respective maximum count rate of the curve.

Figure 4.15 shows orbital modulation curves of the four sources in different intensity states. For each source, the orbital modulation light curves of the high and intermediate intensity states are shown in the top panel, high state points are indicated by blue circles. The low state modulations are shown in the bottom panels. All the orbital modulation curves are normalised by dividing the original light curves by the average count rate calculated over an orbital phase of 0.2 near the peak intensity of the respective orbital modulation curve. The low state ASM light curve for LMC X-4 does not show any orbital modulation.

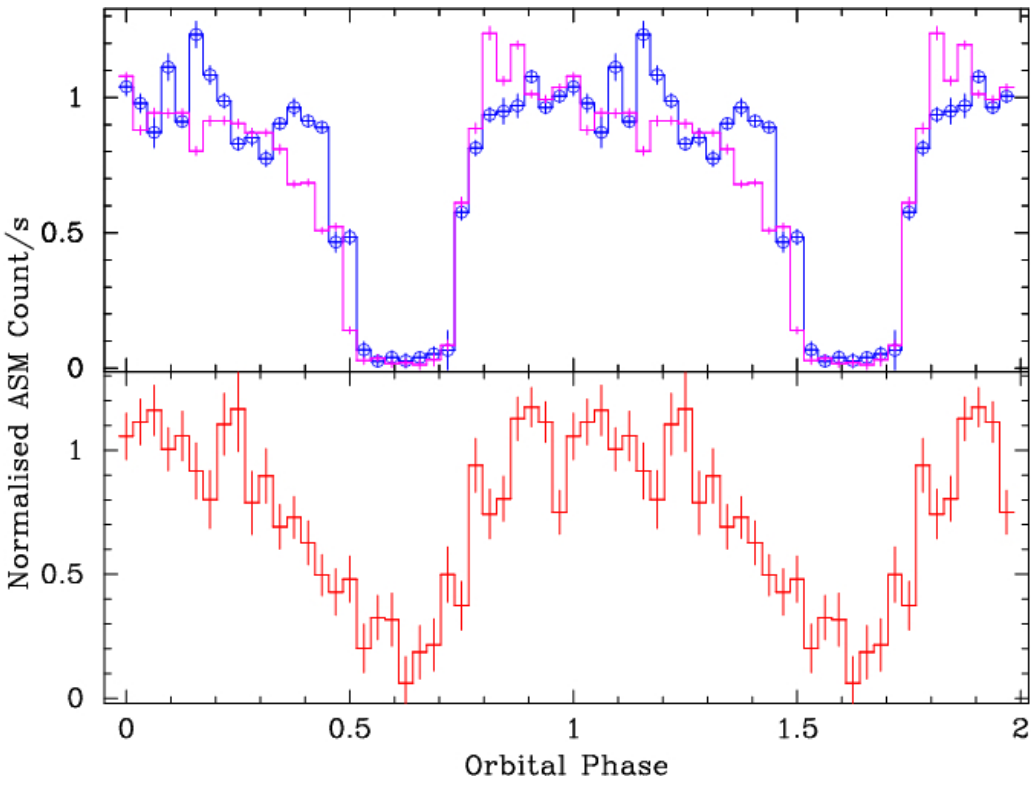

Figure 4.16 Intensity-dependent orbital modulation of the Cen X-3 in hard spectral state during 2000 December to 2004 April. Upper panel plots show high- and intermediate-state orbital modulation, with high-state points being marked with circles. Lowe panel plot shows low-state orbital modulation.

To see if the orbital modulation is similar for both the spectral states of Cen X-3 described in the previous section, all the above analysis was also performed separately for the two spectral states. Figure 4.16a and 4.16b show the orbital modulation curves for soft and hard state of Cen X-3.

4.4.2 Pulsed fraction measurements at different intensity states using the *RXTE*-PCA observations

The pulsation characteristics of Cen X-3 at different intensity levels in the 2-60 keV band are investigated using *RXTE*-PCA data. Cen X-3 was observed by *R*XTE-PCA many times during the years 1996, 1997 and 1998. All these observations have been obtained when Cen X-3 was in the soft spectral state. Eighteen PCA observations were chosen depending on the

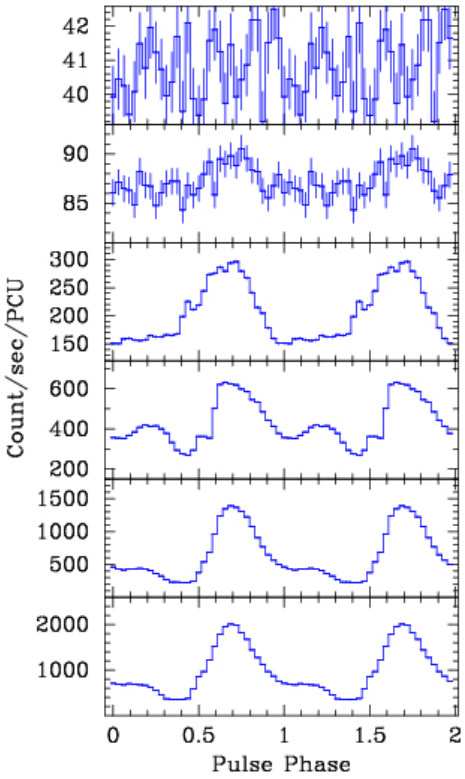

Figure 4.17 Pulse profile of Cen X-3 is shown here in different intensity states of the source. The count rate is per PCU. Hundred consecutive pulses are folded with arbitrary pulse phase and the local spin period to get each of the above pulse profiles.

orbit averaged ASM count rates at that time such that a wide range of X-ray intensity is covered. The 2-60 keV band light curves were obtained from the Standard-1 mode data of the PCA. Background light curves were generated using the background models provided for *R*XTE-PCA by HEASARC and were subtracted from Standard-1 light curves to get the source light curves. The source light curves were first barycenter corrected and then searched for the spin period of the neutron star. We did not detect any pulsations when the orbit averaged ASM count rate of Cen X-3 was less than 0.8 count/sec (equivalent to about 50 count/sec per proportional counter unit) with a 90 per cent upper limit of 0.8 % on the pulsed fraction. The pulse profiles were generated by folding the barycenter corrected light curves by the respective spin period found in that light curve. To avoid smearing of the pulse profiles due to the orbital motion of the pulsar, the pulse profiles were generated from short data segments of duration of a hundred pulses. In Figure 4.17 we have shown six pulse profiles obtained at different

source flux levels including a light curve folded in the low flux state with a period of 4.81 s when no pulses were detected. Figure 4.18 is a plot of the maximum-minimum count rate per Proportional Counter Unit (PCU) against the maximum count rate per PCU for the eighteen pulse profiles. The points marked with the circles are for the pulse profiles shown in Figure 4.17. Epochs of the six PCA observations, pulse profiles from which are shown in Figure 4.17, are marked in the top panel of Figure 4.14. A two component function was fitted to the points in Figure 4.18.

$$F_{\max} - F_{\min} \simeq \begin{cases} 0, & F < F_0; \\ f(F_{\max} - F_0), & F \geq F_0; \end{cases} \tag{4.2}$$

The pulse fraction f of the pulsating component was determined to be 90%, while the unpulsed component grows upto a count rate of $F_0 = 175.5$ per PCU.

As seen in Figure 4.17, apart from the changing ratio of the unpulsed component of the intensity to the total intensity, the pulse shape is also varying from one observation to another. To see whether the pulse shape changes are related to the intensity, we selected three different observations with very similar eclipse subtracted orbit average ASM count rates of 17.12 ± 1.35, 17.52 ± 1.21 and 17.73 ± 1.47. Within these three observations, the pulse shape changed from a double peak profile to a broad single peak profile but the pulsed fraction remained the same. We therefore conclude that while the pulsed intensity of Cen X-3 is related to the total intensity, the pulse shape is independent of the X-ray intensity.

4.4.3 Results from orbital modulation and pulsed fraction studies

As presented in the Figure 4.15, it is found that in all the four sources whose orbital modulation has been studied, the binary modulation of the X-ray intensity shows remarkable dependence on the X-ray intensity state. X-ray eclipses are sharp in the high intensity state which become more gradual in the intermediate state. In the low state, instead of sharp eclipse ingress and egress, there is a smooth intensity variation with orbital phase. It should be noted that though the orbital modulation of LMC X-4 is not detectable in the low state with ASM data, a weak and smooth orbital modulation in the low state of LMC X-4 was clearly detected

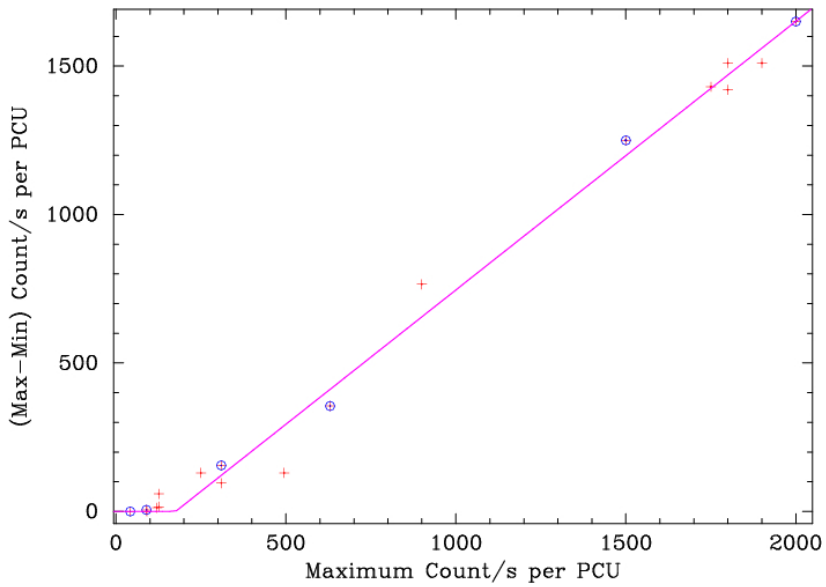

Figure 4.18 Pulsed emission of Cen X-3 is plotted here against the maximum count rate per detector over a range of X-ray flux of the source. The points marked with circles correspond to the pulse profiles shown in 4.17. The solid line in the Figure is a fit to the function given in the text.

earlier with the *BeppoSAX* observations (Naik & Paul 2003). The Her X-1 orbital modulation curves show some pre-eclipse dips (Figure 4.15). In the intermediate state of Cen X-3 the eclipse egress starts earlier in phase by 0.03 compared to the high state as is shown with a vertical dashed line.

The ratio of the X-ray intensity when the source is in eclipse and when it is out-of-eclipse is a measure of the relative scattering efficiency. Only for Cen X-3 there is good enough statistics to compare the ratios. We find that the out-of-eclipse count rates differ by large factor (22.02±0.07, 7.56±0.02 and 1.23±0.02 for high, intermediate and low states respectively) while the in-eclipse count rates of the three states are comparable (0.69 ± 0.07 for high, 0.48 ± 0.03 for intermediate and 0.27 ± 0.03 for low state). The eclipse count rate varies by a factor of only about ∼2.5 while the out of eclipse count rate varies by a factor of ∼18. The ratio of X-ray intensity of Cen X-3 during eclipse and out-of-eclipse is larger in the low state by a factor of 7.0 ± 1.3 compared to the same in the high state. This behaviour is similar to SMC X-1, in which the eclipse count rate was found to be comparable in high and low states whereas the

out-of-eclipse count rate varied by more than a factor of 20 (Wojdowski et al. 1998).

Figure 4.17 shows the spin period pulsations seen in the Cen X-3 light curves at different intensity states. Panel 1 shows Cen X-3 light curve folded at 4.81 s when the average source intensity yielded no clear signal for the spin of the neutron star. The fraction of pulsed emission increases as source intensity increases. Figure 4.18 is a plot of Max-Min count rate per PCU as function of the peak count rate per PCU. Fitting the points with the function 4.2 yields a pulse fraction f of 90 % while the unpulsed component grows upto a count rate of $F_0 = 175.5$ per PCU.

4.5 More insights to Cen X-3 aperiodic Intensity Variations from the QPO studies

From the orbital modulation and pulsed fraction studies of Cen X-3 in its different X-ray intensity states we conclude that the long term X-ray intensity variations of this source are due to variable obscuration of the central X-ray source by an aperiodically precessing warped accretion disk (Raichur & Paul 2008). In this scenario, as the X-ray intensity decreases, reprocessed and unpulsed X-rays from a relatively large scattering medium progressively dominates the observed X-ray intensity. We further investigate this hypothesis using the Quasi Periodic Oscillations (QPO) in Cen X-3 with respect to its intensity state. In the accretion powered X-ray pulsars, the QPOs are understood to be due to inhomogeneities in the inner accretion disk and therefore its frequency is expected to be related to the inner radius of the accretion disk. A correlation between the QPO frequency and X-ray luminosity (and hence mass accretion rate / inner disk radius) has been observed in several transient and persistent X-ray sources which show a large range of X-ray intensity (EXO 2030+375: Angelini, Stella & Parmar 1989, 3A 0535+262: Finger, Wilson & Harmon 1996, XTE J1858+034: Mukherjee et al. 2006, 4U 1626–67: Kaur et al. 2008).

QPOs are known to be present in all types of accreting X-ray pulsars. In most sources it is a transient phenomena and QPOs have been detected in about a dozen out of about a hundred known accreting X-ray pulsars. With a few exceptions (4U 1748-288: Zhang et al.

1996 and XTE J 0111.2-7317: Kaur et al. 2007) the QPO frequency is usually in the range of 40-200 mHz, consistent with it being related to the inner radius of the accretion disk around a highly magnetised neutron star in its bright X-ray state. Previous studies of Cen X-3 power spectrum have shown Quasi Periodic oscillation (QPO) at ~ 40 mHz (Takeshima et al. 1991).

In this section, we present the study of Cen X-3 QPOs and their relation to the source intensity if any. For this we have analysed all the available archival data of the *Rossi X-ray Timing Explorer (RXTE)* proportional courter array (PCA) from the year 1996 to 2000.

4.5.1 Analysis of the RXTE-PCA data of Cen X-3 for Quasi Periodic Oscillations

Cen X-3 was observed extensively by *RXTE*-PCA during 1996-1998 and again for some time in 2000. This covers a wide range of source intensity with maximum orbit averaged ASM count rate of 20.77 to a minimum of 0.52. We have analysed X-ray light curves from all the data available during this period. A total of 525 ks data was obtained from 81 pointings carried out in this period. Very few of the observations were carried out during the eclipse or ingress/egress of eclipse and data collected during these periods were excluded from further analysis. Table 4.5.1 gives details of the observations.

Light curves were extracted from all the observations using Standard-I data which has a time resolution of 0.125 s but no spectral information. Power spectrum was obtained for each of these observations using the Standard-I light curve from data stretches of duration 1024 s. Power spectra from all such stretches within one observation pointing were averaged and normalised such that their integral gives the squared RMS fractional variability and the expected white noise level was subtracted. We have detected QPO features at two different frequencies as described below. However, QPO features were not present in all the data sets. Table 4.5.1 lists mid-times of the 11 segments in which QPOs were detected along with the QPO frequencies. We have detected the earlier reported QPOs around 40 mHz in all of the years although not in every observation. The QPO at 90 mHz was seen only in the observations made in 1996 and never again. The two QPOs 40 mHz and 90 mHz are not seen together in any of the observations. In all the power spectra in which the QPOs were detected, the peak associated

with pulsar spin period was seen very clearly at ~ 0.2 Hz along with several harmonics. As explained in the previous section, pulsations were not detected below a background subtracted count rate of 50 per proportional counter unit with an upper limit of 0.8 % on the pulsed fraction (Raichur and Paul 2008). Some representative power spectra in different intensity states, with and without the QPO features are shown in Figure 4.19 and Figure 4.20.

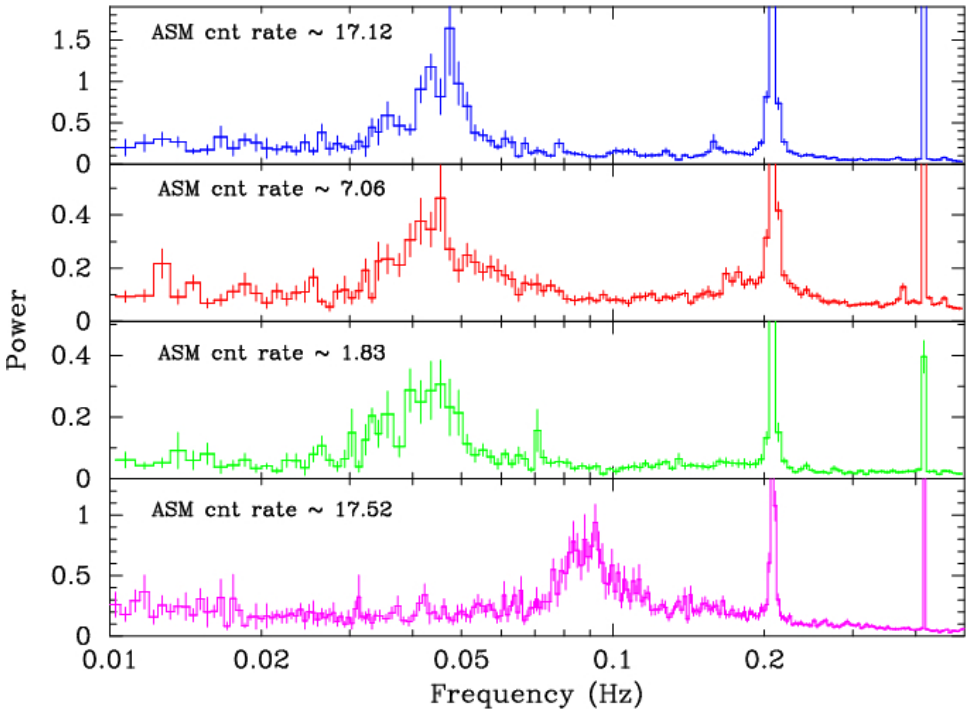

Figure 4.19 Representative power spectra of en X-3 with QPOs are shown here. Top three panels show the 40mHz QPO at different intensity states of Cen X-3. The bottom panel shows the 80mHz QPO seen only during the high intensity state of Cen X-3 in 1996.

One other feature seen in most of the power spectra is a broadening of the fundamental spin frequency peak. To investigate the reason for this broadening we chose the observation which had the highest RMS of the spin frequency broadening feature (Obs. Id P20104, MJD of observation 50508.012 - 50508.713). The total length of this observation is about 60608 s and it gives 51 intervals of 1024 s each. A final power spectrum using 1024 s of data stretches averaged over all the intervals was made and then fitted with the model power spectrum given by Lazzati and Stella (1997). The model power spectrum considers the fact that any aperiodic

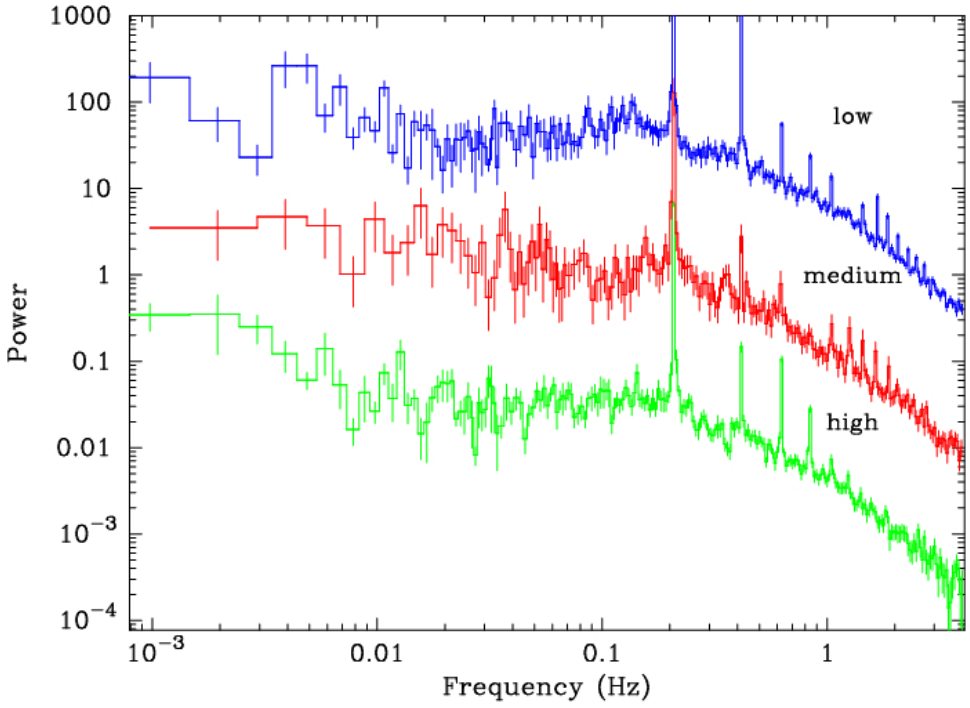

Figure 4.20 Representative power spectra of Cen X-3 at different intensity state without QPOs are shown here. The first and second plots are multiplied by constant numbers for clarity.

variability in the emission from accretion column(s) of a magnetic neutron star should be modulated at the X-ray pulsar period, hence giving rise to a coupling between the periodic and aperiodic variability (Burderi et al. 1997; Menna et al. 2003). The coupling parameter R as defined in the model, is a measure of the degree of coupling between the periodic and the aperiodic variabilities. The effects due to a finite length of the light curve are built into the model (smaller data length broader the spin frequency feature). Fitting this model (equation 5 of Lazzati and Stella 1997) to our power spectrum gives $R \approx 0.64$, similar to the results derived by Lazzati and Stella (1997) using EXOSAT data for Cen X-3. A value of R $\approx$ 1.0 or greater indicates a strong coupling between the aperiodic and periodic variabilities.

In the top panel of Figure 4.21, a plot of the QPO frequency is shown against the 2-30 keV X-ray flux measured with the PCA. To determine the X-ray fluxes we have fitted the X-ray spectra with a simple model consisting of a high energy cut-off power law along with line of sight absorption and iron emission lines. Part of the X-ray light curves that showed pre-eclipse X-ray dips were excluded from X-ray flux determination. Figure 4.23 shows a representative

Table 4.3 List of Observations

Year	Obs Ids	No. of Pointings	Total Durations(ks)
1996	P10063	3	40
	P10132	5	18
	P10133	4	92
	P10134	7	143
	P10144	5	32
1997	P20104	12	32
	P20105	3	26
	P20106	7	14
1998	P30083	10	13.6
	P30084	23	65
2000	P40072	2	50

spectrum of Cen X-3. The PCA X-ray light curves from which the power spectra have been generated represent the instantaneous measurement of X-ray flux over a small period of a few ks. However, even outside the X-ray eclipse, within one orbital period, the X-ray intensity of Cen X-3 varies smoothly by more than a factor of two and rapidly by a factor of upto 4 during the pre-eclipse dips. In a circular orbit, the orbital intensity variation is due to different visibility of the X-ray source and its reprocessing region rather than changing mass accretion rate. Therefore, we have also looked at the QPO frequency against the orbital phase averaged X-ray intensity using data from *RXTE*-ASM. The combined ASM light curve with about 10-20 exposures during each binary orbit of Cen X-3 gives a better estimate of the overall X-ray intensity state of the source. We used the corresponding binary period averaged count rates from ASM light curve to see any dependence of the QPO frequency on the X-ray intensity. The ASM count rates given in Table 2 are obtained from orbital period averaged light curve after removal of data taken during the eclipse. A plot of the QPO frequency with ASM count rate is shown in the bottom panel of Figure 4.21.

We have also carried out an energy resolved QPO analysis from one of the observations (ID P10132) in which strong QPOs were detected at ~ 40 mHz using energy resolved binned mode and event mode data. We extracted light curves with time resolution of 0.125 s in energy bands of 2-4.1, 4.1-6.6, 6.6-9.5, 9.5-13.1, 13.1-16.7, 16.7-20.4, 20.4-25.7 and 25.7-34.8 keV. The energy

Table 4.4 Details of QPOs detected in Cen X-3

Mid Time of Observation (MJD)	ASM Count Rate	QPO Freq (Hz)	QPO width	RMS
50146.7283	17.52 ± 1.21	0.0903 ± 0.0013	0.0091 ± 0.0012	10.95 ± 1.93
50147.3781	17.52 ± 1.21	0.0931 ± 0.0015	0.0094 ± 0.0016	6.21 ± 1.52
50345.6888	17.12 ± 1.35	0.0452 ± 0.0010	0.0068 ± 0.0010	10.88 ± 2.23
50509.5281	13.60 ± 0.92	0.0384 ± 0.0008	0.0113 ± 0.0009	5.11 ± 0.46
50991.4068	10.09 ± 1.80	0.0454 ± 0.0019	0.0125 ± 0.0027	5.71 ± 1.19
50998.7648	17.73 ± 1.47	0.0403 ± 0.0016	0.1281 ± 0.0026	6.19 ± 1.03
50999.7818	17.73 ± 1.47	0.0419 ± 0.0019	0.0048 ± 0.0036	3.43 ± 1.18
51094.9594	1.83 ± 1.21	0.0431 ± 0.0009	0.0069 ± 0.0010	5.93 ± 1.16
51095.9637	1.83 ± 1.21	0.0445 ± 0.0015	0.0064 ± 0.0015	4.93 ± 1.57
51578.9780	8.97 ± 1.19	0.0402 ± 0.0016	0.0051 ± 0.0013	3.75 ± 1.01
51579.9307	7.06 ± 1.06	0.0502 ± 0.0022	0.0101 ± 0.0018	6.49 ± 1.29

resolved analysis of the 40 mHz QPO, as shown in Figure 5 did not reveal any measurable dependence of the RMS fractional variability on energy. Energy resolved analysis for the 90 mHz QPO could not be done as the data from the corresponding observation did not have the required energy and timing resolution in any of the data storage modes.

4.5.2 Results from QPO analysis

Cen X-3 shows transient QPOs clustered at 40 mHz and 90 mHz. The spin frequency feature shows broadening which indicates a weak coupling between the low frequency aperiodic variabilities and the spin frequency. Figure 4.19 shows some representative power spectra at different intensity states of Cen X-3. From this Figure one can clearly see that even though the orbit averaged ASM count rate changes by a factor of 9, the 40 mHz QPO shows no shift in the central frequency. The 90 mHz QPO is seen only during 1996 when the source was in high state. Also the energy resolved analysis of the 40 mHz QPO did not show any dependence of the QPO RMS on the energy range of observation (see Figure 4.22).

The two largely used QPO models are the Beat Frequency model (BFM) and the Keplarian Frequency model (KFM). The BFM explains the QPO as the beat between the spin frequency ν_{spin} and the Keplerian frequency ν_k of the inner accretion disk $\nu_{QPO} = \nu_k - \nu_{spin}$. Thus the

radius of the inner accretion disk according the BFM is given as follows.

$$r_{M,BFM} = \left(\frac{GM_{NS}}{4\pi^2(\nu_{spin} + \nu_{QPO})^2} \right)^{1/3} \tag{4.3}$$

In KFM, the QPO occurs at the Keplerian frequency of the inner accretion disk $\nu_{QPO} = \nu_k$. Therefore radius of the inner accretion disk due to KFM will be

$$r_{M,KFM} = \left(\frac{GM_{NS}}{4\pi^2\nu_{QPO}^2} \right)^{1/3} \tag{4.4}$$

However, in the case of Cen X-3, as the ν_{spin} is larger than the observed QPO frequencies, KFM is not applicable. This is because if the inner accretion disk rotates slower than the neutron star, propeller effect is expected to inhibit accretion of material from the accretion disk. Thus we assume an inner accretion disk origin of the QPOs. The radius of the inner accretion disk around a magnetised neutron star with a mass of $1.4M_{\odot}$ and a radius of 10 km can be approximately expressed in terms of its magnetic moment and X-ray luminosity as (Fran, King & Raine 1992)

$$r_M = 3 \times 10^8 L_{37}^{-2/7} \mu_{30}^{4/7} \tag{4.5}$$

where L_{37} is the X-ray luminosity in the units of 10^{37} erg and μ_{30} is the magnetic moment in units of 10^{30} G cm^3. For disc accretion, often a scaling factor of 0.5 is used with the above expression of r_M. Then the radius of the inner accretion disk would be $R_M = 0.5r_M$. Using equation 4.3 and 4.5, one can express a relation between the QPO frequency and the X-ray luminosity. We have used the value of magnetic field of Cen X-3 to be $B \simeq 3.4 \times 10^{12}$ G (i.e, $\mu_{30} = 3.4$) as reported by Coburn et al. (2002) using the cyclotron absorption line in the X-ray spectrum of Cen X-3. To calculate the X-ray flux we use the source distance of 8 kpc (Krzeminski 1974). Figure 4.21 top panel plots the QPO frequency as a function of the instantaneous flux measured by the PCA spectra. In the same panel we have also plotted the expected relation between QPO frequency and source flux by the BFM. The dotted line is when radius of the inner accretion disk is taken as $0.5r_M$ and solid line is for r_M. The lower panel shows QPO frequency plotted as a function of orbit averaged ASM count rate.

The QPO frequency shows no dependence on instantaneous X-ray flux or orbit averaged X-ray intensity. The QPOs are clustered about two frequencies, 40 mHz and 90 mHz and there is no dependence of the QPO frequency on X-ray intensity even within these two clusters. This tells us that either the observed X-ray flux is not a representative of the mass accretion rate in Cen X-3 or that the origin of the QPO as an inhomogeneity in the inner accretion disk is not applicable to the case of Cen X-3. However, the expression used here for magnetospheric radius (for example if it is considerable larger that r_M in eqn 4.5) can explain the observed QPO frequency at the highest observed X-ray flux state and also be consistent with the proposal that the QPO frequency is insensitive to the measured X-ray flux as the X-ray flux variation is primarily due to disk obscuration.

We also note the other possibility that the QPOS in Cen X-3 may not be due to any material inhomogeneity in the inner accretion disk as is the case for a few other X-ray binary pulsars like A0535+262 (Finger et al. 1996), EXO 2030+375 (Angelini et al 1989) XTE J1858+034 (Mukherjee et al. 2006) and 4U 1626-67 (Kaur et al. 2008). In these transient binary X-ray pulsars, the QPO frequency is well or somewhat correlated with the X-ray luminosity of the source and hence the QPO frequency variations are understood to be due to changes in the mass accretion rate and associated changes in the radius of the inner accretion disk.

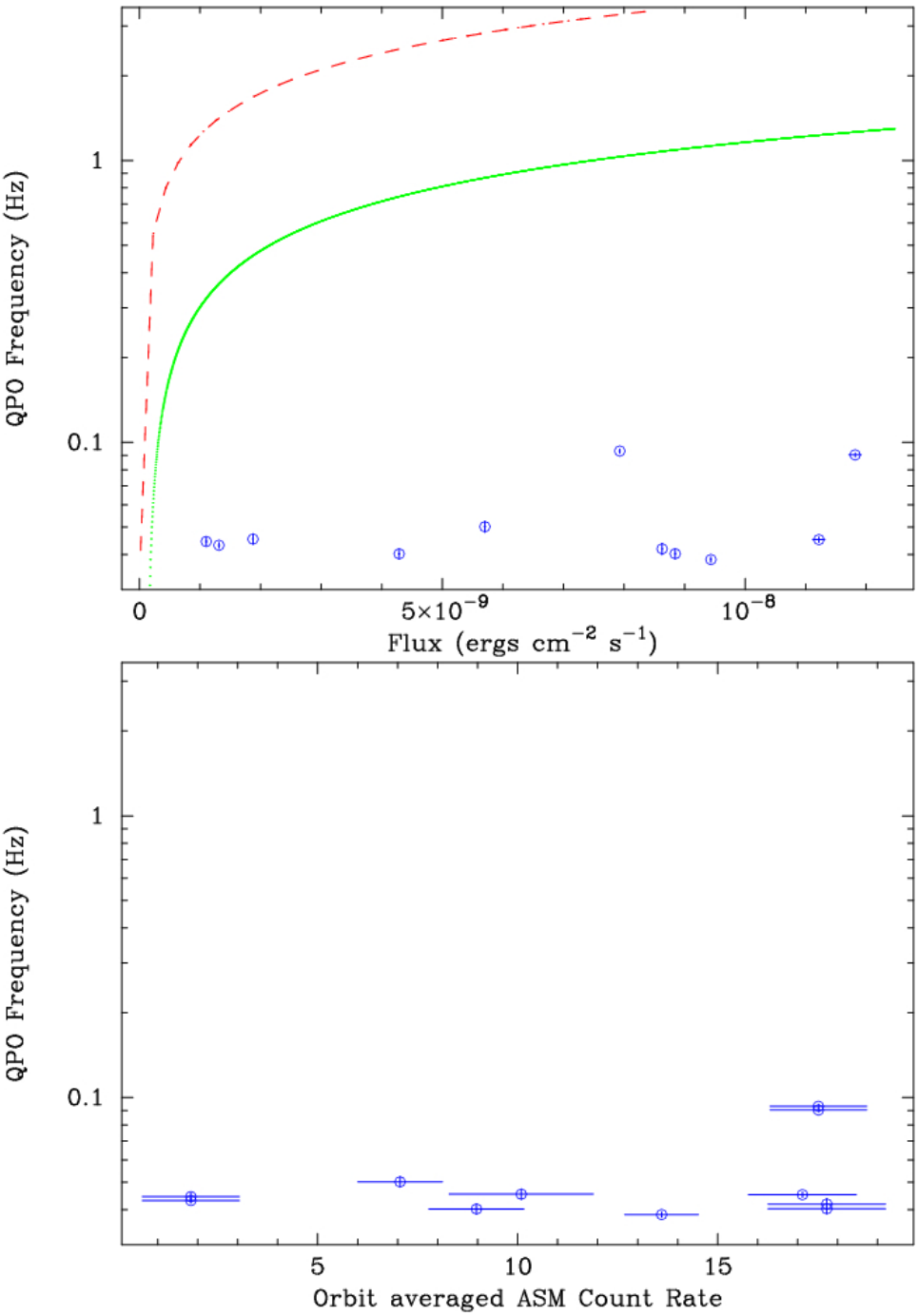

Figure 4.21 Representative power spectra of Cen X-3 at different intensity state without QPOs are shown here. The first and second plots are multiplied by constant numbers for clarity.

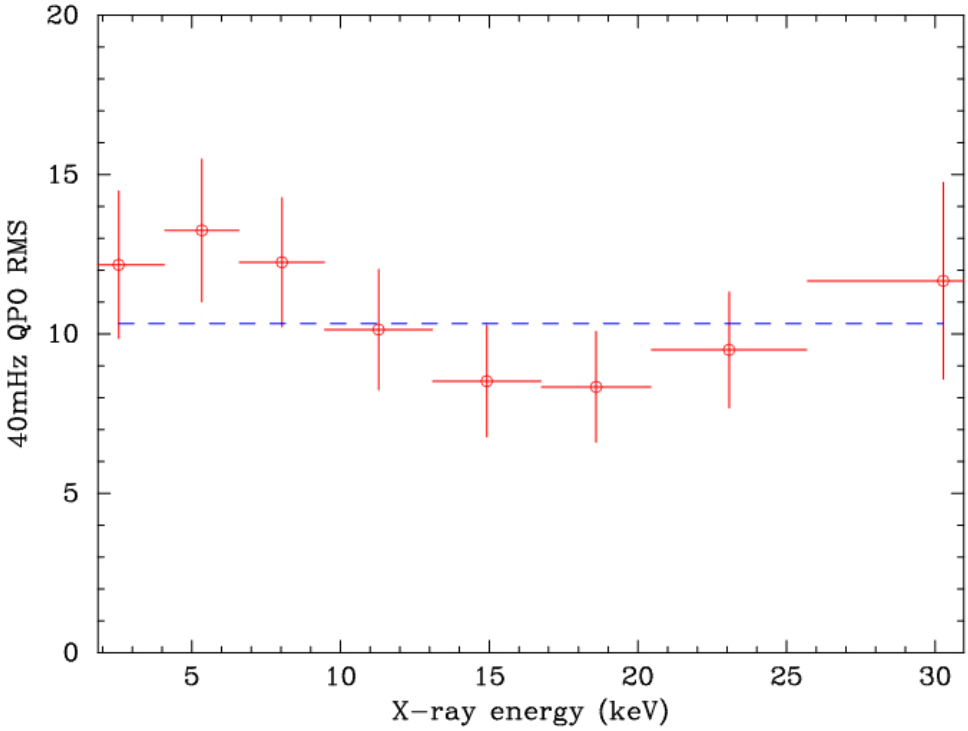

Figure 4.22 Representative power spectra of Cen X-3 at different intensity state without QPOs are shown here. The first and second plots are multiplied by constant numbers for clarity.

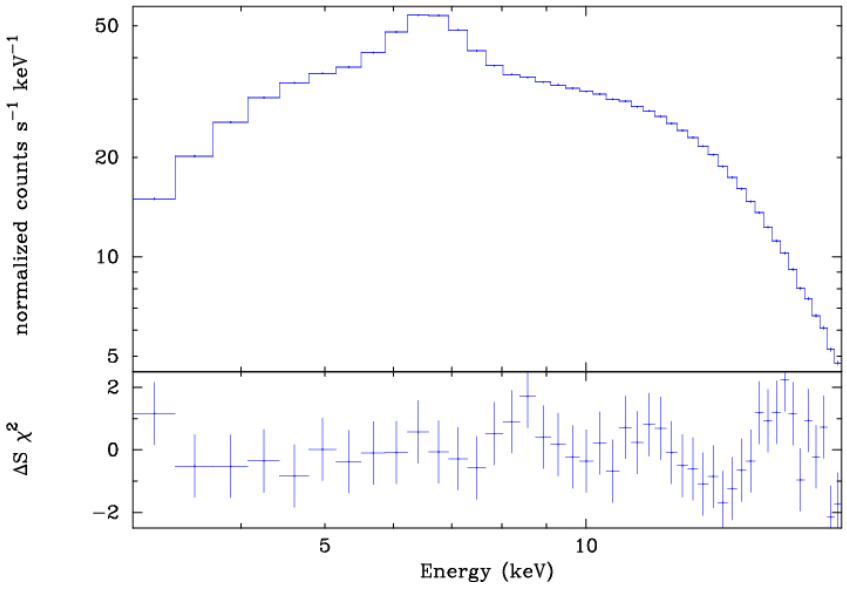

Figure 4.23 Cen X-3 X-ray spectrum. The upper panel is a representative observed X-ray spectrum of Cen X-3. The X-ray spectrum is fitted with a simple model consisting of a high energy cut-off power law along with line of sight absorption and iron emission line.

4.6 Conclusions

From the long term intensity variation studies of Cen X-3 presented in this chapter we can draw the following main conclusions:

1. Cen X-3 long term light curves show intensity variations in all the three energy bands observed by RXTE-ASM. The source switches between the high state and the low state randomly, the low and high states lasting between a few to upto 110 days.

2. There is no periodicity in the long term intensity variations. The peak flux during the bursts is larger by upto a factor of 40 compared to the low state flux.

3. In the high state, Cen X-3 has two distinct spectral modes and during each outburst the source goes through flux changes via only one of the two spectral modes. During any of the individual high states the source never switches between the two spectral modes.

4. There is no significant spectral evolution during each outburst, at least above a flux level of 100 mCrab. All outbursts belong to one of the two spectral modes and have spectral hardness ratio in a very narrow range.

5. There exists a ceiling in the maximum luminosity of the outburst prior to the first change in spectral mode that took place at MJD 51880. This ceiling is very clearly seen in the 5-12 keV ASM light curve (Figure 4.8).

6. The binary orbital modulation of X-ray from Cen X-3 is similar to that seen in the other three accreting X-ray pulsars. From sharp eclipse in high state, it turns to a gradual modulation in the low state. Cen X-3 eclipse egress starts earlier in the intermediate state compared to the high state. These observations indicate a larger emission region in the low state of Cen X-3. The ratio of X-ray flux of Cen X-3 during eclipse and out-of-eclipse is larger in the low state by a factor of 7.0 ± 1.3 compared to the same in the high state.

7. A measurement of the pulsed X-ray flux in different flux states of Cen X-3 is consistent with the X-ray flux having two components, one with a large pulsed fraction and a second unpulsed component that dominates in the low state.

8. We propose that the long term intensity variations in Cen X-3 are mostly due to aperiodic obscuration of the compact source by the accretion disk. The unpulsed X-ray emission from an extended region appears to be due to scattering of the X-rays from the central source by the stellar wind.

9. Cen X-3 shows intermittent QPOs in different frequency ranges namely 40 mHz, and 90 mHz. RMS fluctuation of the 40 mHz QPO is energy independent. A weak coupling is measured between the low frequency aperiodic variabilities and the spin frequency.

10. The presence of the QPOs or the frequency of the QPOs are not related to the luminosity state of the source. The RMS fluctuations associated with the QPOs are not correlated with the luminosity of the source.

Cen X-3 is the brightest accreting X-ray binary pulsar in its high state and one of the brightest X-ray sources in the energy band of *RXTE*-ASM. Its long term aperiodic intensity variations are in stark contrast with the smooth and periodic variations seen in other sources showing superorbital intensity variations, like Her X-1, SMC X-1, and LMC X-4 (see Figure 4.14). Each superorbital period of Her X-1 consists of one main-on phase and one short-on phase separated by two low intensity phases except when the source was in its occasional anomalous low state. LMC X-4 shows a smooth variation in its X-ray intensity during its 30.5 day periodic cycle. SMC X-1 also shows a smooth and almost sinusoidal variation with some scatter within each high state along its quasi-periodic X-ray intensity variations as a time scale of 50-60 days. In the case of Cen X-3, the rise and fall in intensity around the high states which last about 2-8 days, is quite abrupt.

In spite of these difference there is a striking similarity between the X-ray light curve of Cen X-3 and the other three sources being discussed here. The Cen X-3 light curves, especially the 5-12 keV light curve, show a ceiling in the observed maximum flux of the outburst prior to

the first change in spectral mode which is similar to the almost constant peak flux seen in the light curves of Her X-1, SMC X-1 and LMC X-4. This ceiling is broken when Cen X-3 is in the hard state between MJD 51800 and 53100. One way to explain this presence of ceiling is by assuming that it is related to the Eddington luminosity in Cen X-3 for some limited solid angle in the soft spectral mode.

Apart from the aperiodicity of the intensity variations, Cen X-3 also differs from other sources in the spectral evolution of the high states. It does not show spectral variations during individual high states. The scatter in hardness ratio of the two spectral modes of Cen X-3 is very small. Her X-1 for example, shows a large variation in absorption column density over its 35 day superorbital period (Naik & Paul 2003). For Cen X-3 the presence of two spectral modes is more clearly seen in HR-2 and is less obvious in HR-1 (Figure 4.11). This indicates that the harder spectrum is not due to a change in the absorption column density. A change in the column density during the hard state should have had a greater effect in the lower energy band causing a larger difference in the corresponding HR-1 value.

Studying the orbital modulation in different intensity states of Cen X-3 and comparing them with orbital modulation of other sources which show superorbital intensity variations due to obscuration of central X-ray source by a precessing warped accretion disk helps one to understand the Cen X-3 aperiodic intensity variations. In all the four sources Cen X-3, Her X-1, SMC X-4 and LMC X-4, the binary orbital modulation of the X-ray flux shows remarkable dependence on the X-ray flux state (Figure 4.15). X-ray eclipses are found to be sharp in the high flux state which becomes more gradual in the intermediate state. In the low state, instead of sharp eclipse ingress and egress, there is a smooth flux variation with orbital phase. Though the orbital modulation of LMC X-4 is not detectable in the low state of LMC X-4 with ASM data, we note that a weak and smooth orbital modulation in the low state of LMC X-4 was clearly detected earlier with *BeppoSAX* observations (Naik & Paul, 2003). The Her X-1 orbital light curves show some pre-eclipse dips (Figure 4.15). In the intermediate state of Cen X-3 the eclipse egress starts earlier in phase by 0.03 compared to the high state as is shown with a vertical dashed line in Figure 4.15.

The flux dependent orbital modulations of these four sources indicate that at lower flux, an increasing fraction of the observed X-rays are from a larger region, comparable to the size of the companion star. The larger emission region may have different visibility at different orbital phases, leading to the smooth orbital modulation in the low state. Reprocessing of X-rays emitted from the compact star by scattering from stellar wind of the companion star is one likely scenario. However, for Her X-1, which has a low mass companion star, the scattering medium is more likely to be part of the accretion disk and disk outflows than the stellar wind. Zdziarski et al (2007a) have performed a similar analysis of *RXTE*-PCA light curve of the X-ray binary 4U 1820–303 and found a significant dependence of the profile of the orbital modulation on the average count rate. However, in 4U 1820–303, the superorbital modulation is associated with an accretion rate modulation, probably due to third body interaction. Poutanen, Zdziarski & Ibragimov (2008) discovered a superorbital phase dependence of the soft X-ray orbital modulation in Cyg X-1 in its hard spectral state, that is related to the size of a bulge in the outer accretion disk.

The measurement of pulsed X-ray flux as a function of the peak X-ray flux of Cen X-3 as presented in the Figures 4 and 5, is also consistent with a scenario in which the measured X-ray flux has two components. One component is highly variable with a pulsed fraction of about 90% and a second component that is unpulsed. Similar result was obtained for SMC X-1 over a wide range of its measured X-ray flux (Kaur et al. 2007). In the low state, the unpulsed component becomes dominant leading to non-detection of pulses. We also note that in all the four sources mentioned here, the X-ray pulsations (pulse period of $\sim$4.8 s in Cen X-3, 1.24 s in Her X-1, 0.7 s in SMC X-1 and 13.5 s in LMC X-4) have never been detected during the low state of the superorbital period, indicating that most of the radiation observed in low state is probably reprocessed emission from a large region (Wojdowski et al. 1998; Naik & Paul 2003). The non-detection of pulsations is not due to faintness of the sources. Even in the low state, Cen X-3, Her X-1 and SMC X-1 are bright enough for detection of a few percent pulse modulation with the *RXTE*-PCA.

We point out the possibility that the intrinsic X-ray luminosity of the central X-ray source may remain unchanged for a long time. It can be seen in Figure 4.8 that except during the anomalous low state events of Her X-1, the peak luminosity of superorbital modulation of Her X-1, SMC X-1 and LMC X-4 does not change very much and the peak of the 5-12 keV X-ray luminosity of Cen X-3 also has a ceiling (see Figure 4.8). Though the results presented here indicate that the different flux states of Cen X-3 are largely due to varying degree of obscuration, as is the case with Her X-1, SMC X-1 and LMC X-4, we cannot completely rule out some contribution to the variability from a varying mass accretion rate, especially the variations associated with spectral change. But as shown in Figure 3, even during the hard spectral state of Cen X-3 from December 2000 to April 2004,the orbital modulation light curve indicate an extended X-ray source at low flux level.

The observed QPO properties of Cen X-3 are in agreement with the scenario in which the long term X-ray intensity variation is due to change in obscuration by an aperiodically precessing warped accretion disk. The lowest and the highest 3-30 keV X-ray flux at which the 40 mHz QPO feature is seen are 1.1×10^{-9} and 1.18×10^{-8} erg cm^{-2}s^{-1} respectively. Assuming a distance of 8 kpc (Krzeminski 1974), these correspond to X-ray luminosity of $L_{low} = 2.64 \times 10^{37}$ erg s^{-1} and $L_{high} = 2.83 \times 10^{38}$ erg s^{-1}. If the observed X-ray luminosity represents the true X-ray luminosity and a proportional mass accretion rate of Cen X-3, the inner accretion disk radius (R_M) will approximately vary between 3×10^8 cm and 1.5×10^8 cm. We note that the corotation radius of Cen X-3 ($P_{spin} \sim 4.8$ s) is $4.7 \times 10^8 cm$, larger than the inner disk radius for the lowest X-ray luminosity, and the QPO detections are outside a possible propeller regime. In the top panel of Figure 4.21, we have shown the expected QPO frequency against the measured X-ray for a source distance of 8 kpc. It is obvious from the Figure that the QPO frequency of Cen X-3 does not have the flux dependence as expected in the beat frequency model. The nearly constant QPO frequency (ignoring the rare 90 mHz feature) is indeed consistent with the variable obscuration due to a warped precessing accretion disk. Hence mass accretion rate and thus the inner accretion disk radius of Cen X-3 are not highly variable, explaining why the source produces a nearly constant QPO at 40 mHz.

One study which could give us more insight would be to study the emission lines from neutral, H-like and He-like iron atoms in the photoionised circumstellar material. Such spectral observations done during the eclipse ingress and egress of the source would give us knowledge of the distance at which the lines are produced. Measurements carried out at different intensity states of the source will tell us if the observed X-ray intensity is a true measure of the X-ray luminosity and the ionization parameter.